RSC Advances

PAPER

View Article Online
View Journal | View Issue

Cite this: *RSC Adv.*, 2022, **12**, 22342

Molecular insights into the 'defects' network in the thermosets and the influence on the mechanical performance†

Fugui Zhao, Haobo Zhang, Dujuan Zhang, Xiaomu Wang, Dingxuan Wang, Junying Zhang, Jue Cheng* and Feng Gao*

The introduction of 'defects' to the thermoset crosslinking network is one of the most applicable strategies for improving the modulus and toughness simultaneously. However, the reinforcement effect disappears when the 'defects' proportion exceeds the threshold. The speculated mechanism was that the aggregation and entanglement of the 'defects' chains changed the matrix topology, making the stacking structure more compact. However, the 'defects' are hardly directly observed in the experiment. As the result, the relationship between the 'defects' proportion and the package state of the matrix, and the effect on the material's mechanical performance was not explored. Herein, the network of bisphenol-A diglycidyl (DGEBA) with diethyltoluenediamine (DETDA) as the hardener was constructed using MD simulation, and *n*-butylamine was decorated on the matrix by replacing a proportion of DETDA acting as the 'defects'. The results indicated that the aliphatic chains aggregated and entangled at a low concentration, occupying the voids in the rigid aromatic crosslinking structure, thus lowering the free volume. The strong non-bonding interactions drew the matrix segments close together, thus reinforcing the resin. However, the microphases formed by the aliphatic chains no longer filled the voids but created a new free volume and loosened the network when the content increased, which reduced the mechanical performance of the material. The experimental results were consistent with the findings in the simulations. The moduli of the resin increased with the increase in the *n*-butylamine content first and then declined. The maximum moduli of the thermosets was 3.4 GPa in S_{30}, which was about 25% higher compared with the control; the corresponding elongation at break was 8.9%, which was about 46% improved compared with the control.

Received 16th May 2022
Accepted 23rd June 2022

DOI: 10.1039/d2ra03099c

rsc.li/rsc-advances

Introduction

Thermosets with outstanding mechanical properties, anticorrosion ability, and processing fluidity are widely used as structural components in a variety of fields, such as aerospace, aircraft, and automotives.[1] It is one of the most primary targets of researchers to design and fabricate the thermosets with high strength and high toughness simultaneously; however, it remains a challenge.[2] The moduli of cured thermosets were dominated by the 3D network structure, and it was one of the most straightforward strategies to enhance the thermosets' moduli by increasing the crosslinking degree.[3] However, the dense crosslinking network limited the segments motion, thus greatly reducing the toughness of the material.[4] As the result, there is a trade-off between the strength and toughness in the thermoset design and fabrication. Strategies were employed to reinforce the thermosets with lesser impact to the toughness in the recent decades. The participation of the elastomer particles was able to toughen the epoxy resin; however, the negative effects on the mechanical performance, such as the glass transition temperature (T_g), moduli, and viscosity, were not totally eliminated.[5–9] The inducing of graphene[10] and carbon nanotubes[11] was able to improve the moduli without affecting the toughness and T_g. However, it was difficult to uniformly disperse the fillers with the nanoscale dimension into the thermosets.[12]

Beside the participation of fillers, constructing the 'defects' in the thermoset matrix by designing or adjusting the network topology could also vary the physical and chemical properties.[13–15] Our previous works introduced the aliphatic dangling chains as the 'defects' into the epoxy network, and the tensile strength was enhanced from 52.3 MPa to 98.5 MPa; the elongation at break was increased from 2.7% to 6.1%, and the tensile modulus was improved from 2.9 GPa to 3.1 GPa.[15–17] Sharifi *et al.* added a solvent into the polymer matrix as the 'defects', thus increasing the volumetric energy capacity based

Key Laboratory of Carbon Fiber and Functional Polymers, Ministry of Education, Beijing University of Chemical Technology, Beijing 100029, People's Republic of China. E-mail: gaofeng@mail.buct.edu.cn; chengj@mail.buct.edu.cn

† Electronic supplementary information (ESI) available. See https://doi.org/10.1039/d2ra03099c

on the Reactive Encapsulation of Solvent/Drying theory (RESD).[13] The results showed that the toughness of the cured matrix was increased without a significantly change in the glassy moduli and T_g. Sharifi *et al.* then rearranged the polymer network heterogeneously into the nanoscale and created the 'defects' *via* the partially reacted substructure (PRS) processing method without changing the chemical composition.[14] The results demonstrated the significantly improved fracture toughness, and the thermal and mechanical performance. Brian *et al.* constructed the 'defects' in the anhydride-cured epoxy matrix by introducing polydicyclopentadiene, which led to an increase in the strength and toughness simultaneously.[18] Microphase separation was obtained after the introduction of the 'defects', which was supposed to toughen the thermosets; however, the corresponding strengthening mechanism is not clear.

In our previous work, it was speculated that the molecular chains involved in the 'defects' aggregated and entangled, thus changing the matrix topology and making the stacking structure more compact.[15,16] The relationship between the intermolecular interactions and mechanical performance was studied in the recent decades. Varley *et al.* suggested that the modulus was mostly dependent on short-range motions rather than long-range microstructural variations, indicating that the crosslinking degree may not dominate the moduli.[19] Morel *et al.* also pointed out that the dominating factor influencing the moduli was not the crosslinking density but the cohesive energy which, was reflected by the change in the free volume.[20] Vallo *et al.* compared the moduli of amine-cured epoxy resins prepared with different stoichiometric ratios; the results showed that the moduli were dominated by the packing density and sub-vitreous relaxations.[21] However, the influence of the free volume change caused by the 'defects' toward the mechanical performance is yet to be systematically studied as the 'defects' were difficult to be directly observed and quantified in the experiment because of the complexity and ambiguous decisive factors of the 3D network.

Molecular dynamics (MD) simulation was employed in this work for exploring the relationship between the 'defects' proportion and the package state of the matrix, and the effect on the material's mechanical performances. The MD simulation, as a theoretical calculation method for polymer simulation, has been proved to be effective in predicting the material properties in various fields, such as physics, chemistry, biology, and engineering.[22–26] The MD simulation showed the feasibility in the epoxy system. Yarovsky *et al.* developed the static methodology and constructed the epoxy crosslinking models with the help of MD simulation.[27] Varshney *et al.* established the cured epoxy structure using MD simulation and predicated the mechanical properties successfully.[28] As a result, the MD simulation was recognized as a powerful and accurate tool to study the relationship between the structure and the properties of the epoxy systems. Li *et al.* explored the relationship between the evolution of the network topology and the glass transition temperature, yield stress, and stiffness using the MD simulation.[29] Masoumi *et al.* monitored the epoxy resins' crosslinking structure with the help of MD simulation based on the accurate calculation of the glass transition temperature, coefficient of thermal expansion, and elastic constants.[30] In the presented work, a rigid aromatic resin matrix was constructed using DGEBA with DETDA as the hardener. The flexible aliphatic *n*-butylamine chains were decorated on the DGEBA-EDTDA network, replacing a proportion of DETDA acting as the 'defects'. The molar ratio between the epoxy group and the $-NH_2$ groups was kept at 2 : 1 constantly in all the formulations. Li *et al.* demonstrated that the MD simulation could predict the mechanical performance of the DGEBA-DETDA system accurately.[31] The radial distribution function (RDF) of the system was recorded to evaluate the aggregation. The cohesive bonding energy, X-ray spectra, and free volume of the system were determined for the quantitative evaluation of the 'defects'. The tensile strength and glass transition temperature were determined, and the relationship between the 'defects' and the mechanical performance was constructed and discussed.

Results and discussion

The formulation and abbreviation of each sample is demonstrated in Table 1. The rigid 3D network was constructed *via* the crosslinking of DGEBA with tetrafunctional DETDA. The flexible bifunctional *n*-butylamine was then induced into the system, replacing DETDA and creating the 'defects' in the matrix. The tensile moduli of all the samples were simulated with 1% deformation, and are plotted in Fig. 1a. Yang *et al.* reported that the MD simulation was able to predict the tensile moduli accurately with a small deformation rate.[26] The tensile moduli of the net DGEBA-DETDA thermosets (S_0) calculated by the dynamic simulation was about 3.6 ± 0.12 GPa with a transfer rate more than 90% in this work. Also, the corresponding experimental value was 2.7 ± 0.10 GPa, which was lower than the simulated one as the crosslinking degree was difficult to reach the simulation level under the real experimental condition. The simulated tensile moduli of S_0, S_{10}, and S_{20} showed no significant difference when *n*-butylamine was induced with low concentration. However, the tensile moduli increased to 4.1 ± 0.07 GPa, 4.7 ± 0.05 GPa, and 4.2 ± 0.02 GPa for S_{28}, S_{30}, and S_{32}, respectively, with the content of *n*-butylamine. The experimental tensile strength with 1% deformation showed a similar changing trend as that of the simulated values, and the corresponding values for S_{28}, S_{30}, and S_{32} were 3.3 ± 0.18 GPa, 3.4 ± 0.22 Gpa, and 3.5 ± 0.24 GPa, respectively. However, the

Table 1 Number of molecules in different systems in the MD simulation

System	DGEBA	DETDA	*n*-Butylamine
S_0	400	200	0
S_{10}	400	195	10
S_{20}	400	190	20
S_{28}	400	186	28
S_{30}	400	185	30
S_{32}	400	184	32
S_{40}	400	180	40

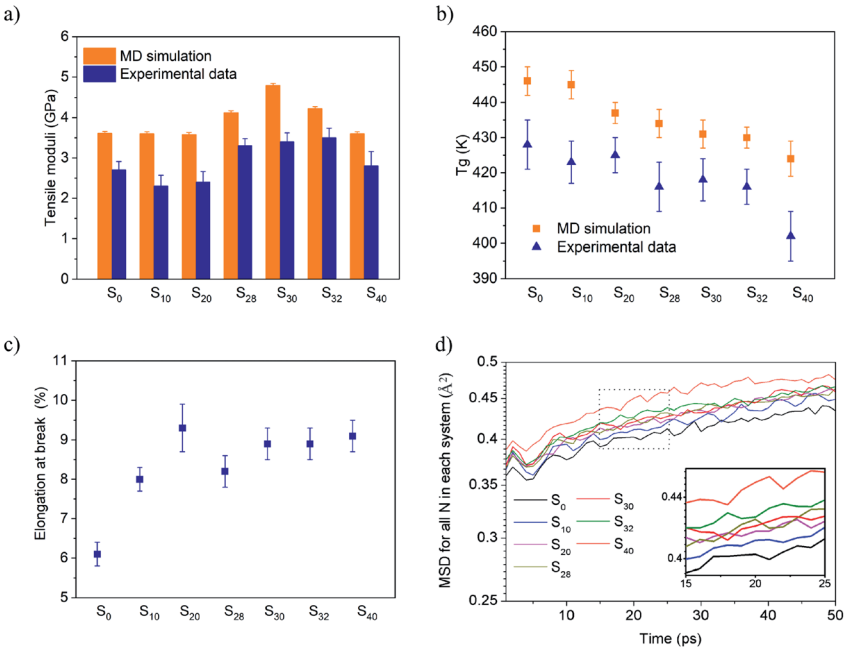

Fig. 1 Experimental and simulated mechanical and thermal performance of the thermosets, (a) the experimental and simulated tensile moduli; (b) the experimental and the simulated T_g; (c) experimental elongation at break; (d) MSD for all the N in each system.

simulated and experimental tensile moduli for S_{40} reverted back to 3.6 ± 0.05 GPa and 2.8 ± 0.36 GPa, respectively, indicating that the 'defects' only reinforced the thermosets at a low concentration. The T_g was defined as the intersection of the bilinear fitting of the volume–temperature data points in the MD simulation[26] (the fitting curves are presented in the ESI section†), and is demonstrated by Fig. 1b. The T_g decreased gradually from 446 ± 4 K for S_0 to 424 ± 5 K for S_{40} with the increase in the *n*-butylamine content. The experimental T_g was measured by DSC and plotted, as shown in Fig. 1b, which followed the same changing trend of the simulated values, however, significantly lower. The reason was that the cooling rate of DSC measurement was 10 K min^{-1}, which was about 10 orders lower than that of the MD simulation (10 K/50 ps), and the glass transition lagged in the DSC measurement. The toughness of the thermosets was evaluated by the elongation at break, which was plotted as shown in Fig. 1c. The S_0 sample broke with only 6.1 ± 0.3% elongation due to the rigid 3D network structure of DGEBA-DETDA, and the stress–strain curves were presented by the ESI section.† The elongation at break increased with the introduction of *n*-butylamine, which became 8.1 ± 0.4% and 9.3 ± 0.6% for S_{10} and S_{20} respectively, and remained about 9% for S_{28} to S_{32}. Interestingly, S_{20} showed a significantly higher elongation at break than that of S_{28}, and the proposed explanation was the compact network of S_{20} caused by the entanglement of the aliphatic chains, which is discussed in the next section. The MD simulation can hardly predict the elongation at break due to the high deformation rate. However, the toughness could be roughly reflected by the mean square displacement (MSD) of the atoms in the matrix.[26,34–36] Fig. 1d presented the MSD of nitrogen in these systems. Fig. 1d inset clearly shows that the flexibility of the N atom increased when a portion of the rigid aromatic network was replaced by the aliphatic chains, showing an increase in the toughness caused by the 'defects', which was roughly consistent with the experimental results. The 'defects' were generated in the matrix as the rigid aromatic DETDA and flexible aliphatic *n*-butylamine were at opposite ends. At the same time, the crosslinking degree of the thermosets decreased from 2288 mol m^{-3} for S_0 to 2067 mol m^{-3} for S_{40} when the tetrafunctional DETDA was gradually replaced by the bifunctional *n*-butylamine. As a result, the tensile moduli should decrease. However, both the simulated and experimental results showed that S_{28}, S_{30}, and S_{40} were reinforced and toughened significantly and simultaneously when *n*-butylamine was introduced. Also, the reinforcement effect disappeared when the 'defects' content increased. All these results were consistent with the finding of our previous work that the low concentration of the 'defects' was able to reinforce and toughen the thermosets simultaneously.

The behavior of the atoms from *n*-butylamine was explored *via* MD simulation in order to discover the reinforcement mechanism of the 'defects' in the thermosets. The RDF described the position characteristics of the carbon and nitrogen from *n*-butylamine in the epoxy resin. The relationship between each parameter was described by eqn (1),[30] where χ_α and χ_β represent the mole fraction of α and β atoms, respectively, N is the number of atoms in the system, ρ is the system density, and δ is the number of atoms existing in a specified area.

$$\chi_\alpha \chi_\beta \rho g(r) = \frac{1}{N} \sum_{i=1}^{N_\alpha} \sum_{j=1}^{N_\beta} \delta_{(r-r_i+r_j)} \quad (1)$$

$g(r)$ represents the probability of finding an atom with the same characteristic within the r radius for each atom in the amorphous cell. As presented in Fig. 2b–g, all the $g(r)$ curves remain zero in the beginning due to the volume exclusion effect, and fluctuations were reflected by all the curves because of the rotation of the C–C bonds of *n*-butylamine.[34] The definition of N, C1 to C4 was demonstrated by Fig. 2a, and C1 represented the terminal carbon of *n*-butylamine. The r value when the $g(r)$ became non-zero is C1, which was abbreviated as r_{min}(C1) for short. The r_{min}(C1) in the S_{10} system was 13.325 Å, which was longer than the cut-off radius of van der Waals' interaction (12.5 Å), indicating that there was no interaction between the single-ended aliphatic amine chains in the S_{10} formulation. The r_{min}(C1) became less than 12.5 Å when the *n*-butylamine content increased and reached about 3.7 Å for S_{40}. Similar trends were reflected by C2, C3, C4, and N in each formulation. The above results indicated that the single-ended aliphatic amine chains were drawn to each other in the defects network when the *n*-butylamine content was increased. The $g(r)$ values for all the atoms in S_{10} fluctuated after reaching the r_{min} and showed a similar trend with that of the net *n*-butylamine system, which is presented in the ESI section.† The peaks were reflected by $g(r)$ in the S_{20} system once reaching r_{min}, and were significantly higher than the fluctuations. This trend became more obvious in S_{28}, S_{30}, and S_{32} systems, where the $g(r)$ values were almost zero after the peaks. The peaks were also reflected in S_{40}; however, they were no longer significantly higher than the fluctuations. It was reflected that *n*-butylamine was random decorated on the matrix, and the aliphatic chains rotated freely in S_{10}. However, the aliphatic chains were packed more regularly when the concentration of *n*-butylamine increased; thus, the $g(r)$ became negligible once the significant peaks appeared after the r_{min} in S_{20} to S_{32}. The constraint to the aliphatic chains was weakened and disappeared when the *n*-butylamine concentration increased. The RDF results indicated that the packing state of the flexible aliphatic chains (the 'defects') in the rigid aromatic thermosets matrix was greatly influenced by its concentration. The RDF of S_{40} at 400 K is presented by Fig. 2h,

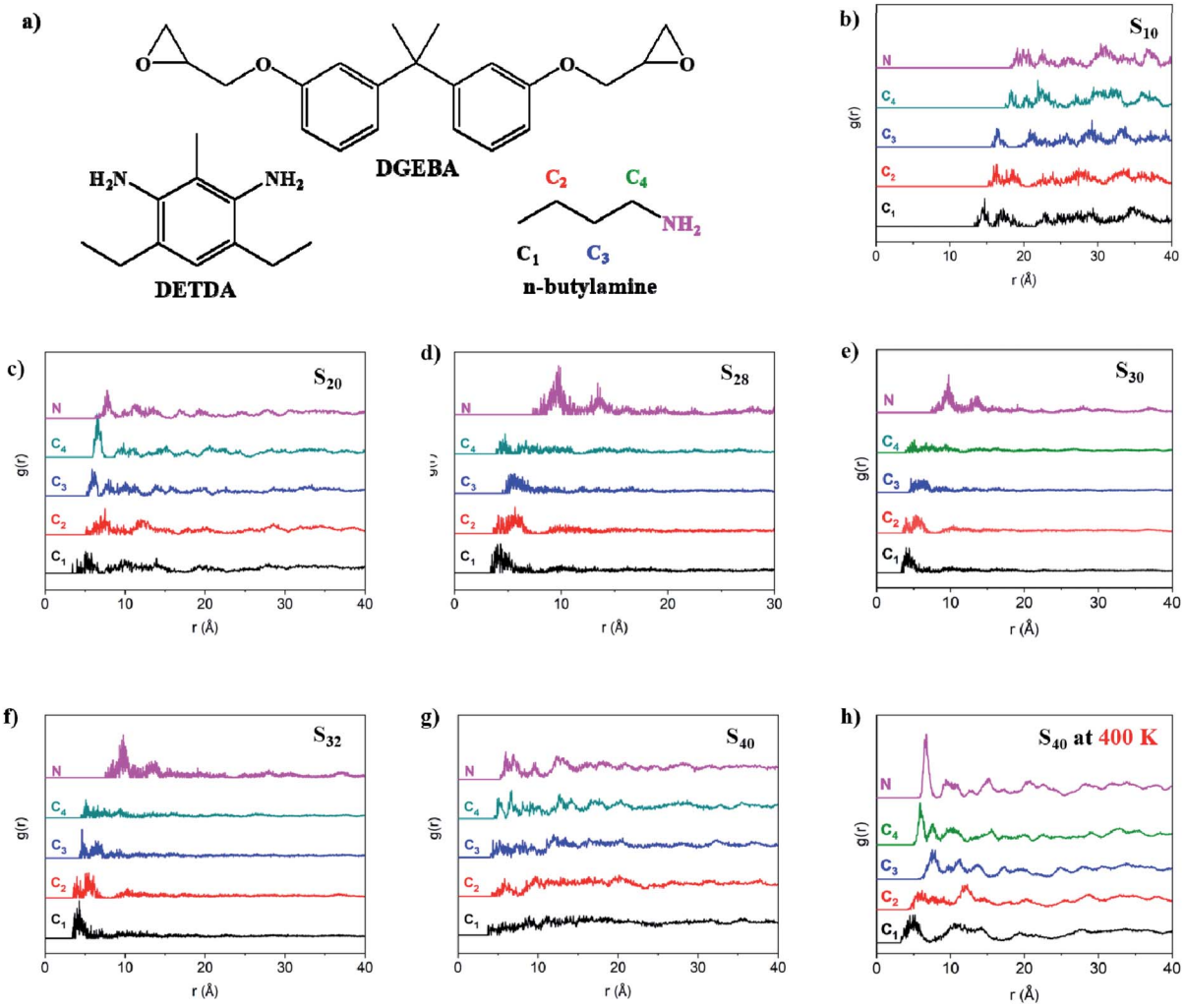

Fig. 2 Schematically demonstration of the thermosets, and the RDF of all the atom from *n*-butylamine for each formulation. (a) Schematic demonstration of the thermosets, (b–g) MDS of all the atom from *n*-butylamine for S_{10} to S_{40}, respectively; (h) the RDF for S_{40} at 400 K.

indicating that the increase in the temperature was able to promote the aggregation of the aliphatic chains. This could be one of the reasons behind the decrease in the T_g caused by the 'defects', where the aliphatic chains moved inversely during the increasing in the temperature.

As indicated by Morel *et al.*, the free volume plays an important role in affecting the mechanical performance of the thermosets.[20] A probe atom with 0.8 Å radius was employed in our model for the detection of the free volume and the calculation of the distribution.[31] The free volume void with irregular shape for each formulation was calculated and described as the volume-equivalent sphere, as shown in Fig. 3. The free volume voids' size distribution in the range from 0 to 7 Å is presented in Fig. 3c. The proportion of the large voids (r > 4 Å) disappeared after the introduction of *n*-butylamine in S_{10}, and that of the medium voids (2 Å < r < 4 Å) increased significantly. The number of large voids kept decreasing in S_{20}, where the proportion of the small voids (r < 2 Å) increased. The large voids almost disappeared in the S_{30} system, and the portion of small voids increased significantly. However, the large voids appeared again when the concentration of *n*-butylamine kept increasing. Also, the distribution shifted to the right side in S_{40}, indicating the increase in the voids' dimension in this case. This trend is reflected clearly in Fig. 3a, which presents the voids' size cumulative distribution. The cumulative portion of the voids for S_{30} was significantly higher than that of S_0 to S_{20}. The number of voids with different size for all the formulations is plotted in Fig. 3b; the distribution shifted from the right side to the left when the formulation changed from S_{10} to S_{30}; however, it turned to the right side again in S_{40}. The total free volume and the corresponding fraction of the thermosets for all the formulations was calculated and is presented in Fig. 3d and e, respectively. The simulation results indicated that the large voids in the rigid aromatic thermosets matrix were occupied with the introduction of the aliphatic chains leading to the reduction of the free volume. However, large voids appeared again when the defects concentration increased. Hypothesis was raised that the *n*-butylamine chains showed no significant influence on the free volume of the thermosets at low concentration due to the lack of interactions between the aliphatic chains (as presented by the RDF simulations). These 'defects' chains aggregated and entangled when the concentration increased, and occupied the large voids in the matrix. However, the aggregation of the 'defects' was too large to fit the voids and generated a new free volume with an increasing concentration of *n*-butylamine.

The intermolecular cohesive energy was examined and is compiled in Table 2 in order to verify the raised hypothesis. The results indicated that the intermolecular interaction was greatly affected when *n*-butylamine was induced. The total cohesive energy for the DGEBA-DETDA was 8283 ± 75 kcal mol^{-1} and 8211 ± 76 kcal mol^{-1} for S_{10}, thus showing no significant change. This value increased gradually to 8333 ± 72 kcal mol^{-1} for S_{20} and 8761 ± 71 kcal mol^{-1} for S_{30}, respectively; however, it decreased to 7754 ± 75 kcal mol^{-1} for S_{40}. The electrostatic energy for the system kept decreasing with an increase in the aliphatic chains' proportion as the regular network structure was gradually destroyed by the defects. However, the van der Waals energy of S_{10}, S_{20}, and S_{30} showed a significant increase compared with that of the control and reverted back to 1376 ± 39 kcal mol^{-1} for S_{40}. The calculation of the cohesive energy was consistent with the RDF simulation and verified the hypothesis.

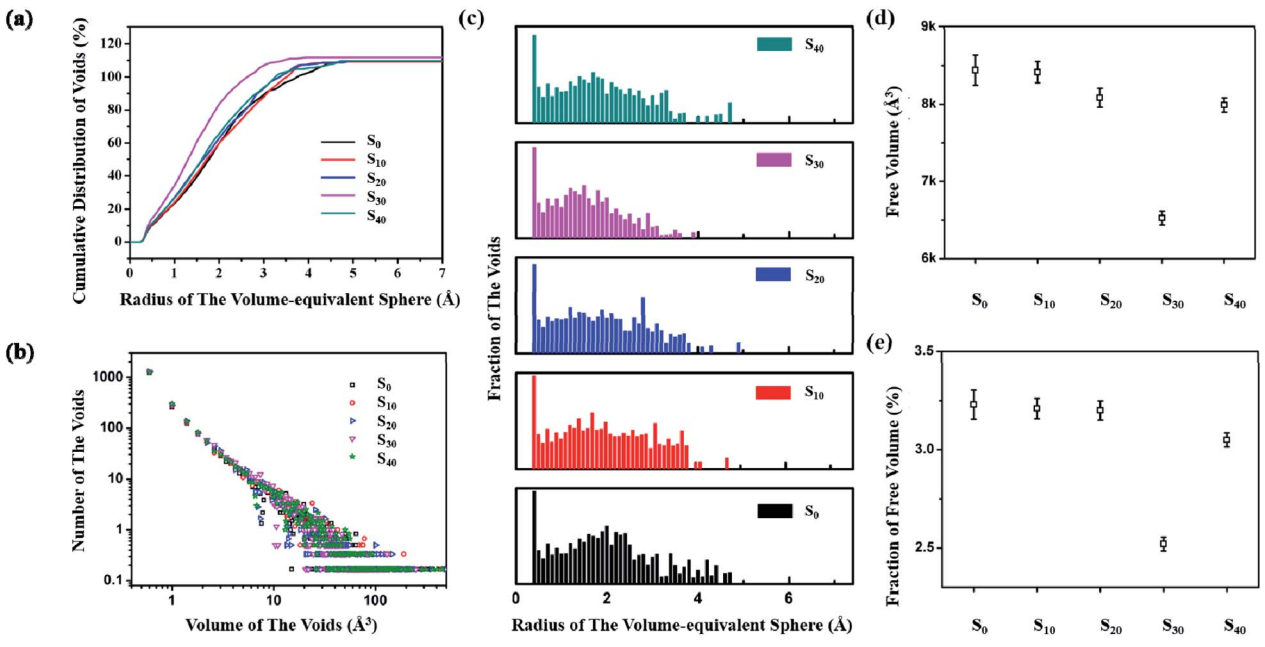

Fig. 3 The simulated free volume. (a) The cumulative distribution; (b) the distribution of the voids number with the change in the voids volume; (c) the radius of the voids and the distribution for each formulation; (d–e) the free volume and the fraction of the free volume in each system.

Table 2 The simulated cohesive energy in each system

System	Cohesive energy, kcal mol^{-1}	van der Waals energy, kcal mol^{-1}	Electrostatic energy, kcal mol^{-1}
S_0	8283 ± 75	926 ± 34	7357 ± 43
S_{10}	8211 ± 76	980 ± 41	7231 ± 37
S_{20}	8333 ± 72	1339 ± 36	6994 ± 41
S_{30}	8761 ± 71	2175 ± 27	6585 ± 44
S_{40}	7754 ± 75	1376 ± 39	6377 ± 34

No significant intermolecular interaction was presented by the aliphatic chains when the concentration was low as the van der Waals energy showed no significant change in S_{10}. However, the aromatic network was destroyed by the introduction of these 'defects' as the electrostatic energy kept decreasing with the increase in the *n*-butylamine proportion. The 'defects' chains begun to interact in S_{20} as the distance between the chains was within the cut-off radius of van der Waals interaction, leading to a significant increase in the van der Waals energy. This trend became more obvious in S_{30} where the van der Waals energy was 2175 ± 27 kcal mol^{-1}, almost twice that of the control. However, the aggregation of the aliphatic chains was weakened in S_{40}.

Interestingly, the change in the tensile moduli of the sample sets followed the variation in the 'defects' chain aggregation. The packing topology of the epoxy matrix was explored in order to clarify the relationship between the participation of the 'defects' and the mechanical performance. Fig. 4a demonstrated the RDF of all the N atoms (including the N from *n*-butylamine and DETDA), which reflected the change in the crosslinking topology. The *r* value corresponding to the peak of $g(r)$ reflected the mean distance between the two N atoms in the amorphous cell. The curves of S_{10}, S_{20}, and S_{40} hold the same position compared with the control. However, the $g(r)$ peak of S_{30} shifted to the left significantly, which showed the more compact 3D network structure compared with the control. The X-ray scattering spectrum was simulated and is presented in Fig. 4b. The wavelength was set as 1.54178 Å with the 2θ ranging from 5 to 45°. The X-ray spectrum could help to qualitatively identify the average distance between the molecular segments in the system. No diffraction peak was presented in all the formulations, which indicated that the thermosets with 'defects' in this simulation remained amorphous. The spectrum shifted to the right with the increase in the *n*-butylamine proportion. However, the spectrum shifted to the left when the formulation changed from S_{30} to S_{40}. The X-ray simulation was consistent with the RDF, where the compact degree of the crosslinking network increased with the introduction of the 'defects' aggregation; however, it decreased when the 'defects' proportion exceeded the threshold value. As a result, the closely packed network structure led to higher tensile moduli. This could explain the reason that the low proportion of the 'defects' in the matrix could reinforce and toughen the thermosets simultaneously.

The behaviors of the 'defects' in the thermoset matrix could be explained based on the above simulated and experimental results, which are demonstrated in Fig. 5. *n*-Butylamine ($f = 2$) replaced DETDA ($f = 4$), reducing the crosslinking degree. As a result, the resin showed a decreasing T_g and increasing elongation at break. The flexible aliphatic chains acted as the 'defects' when decorated in the rigid aromatic crosslinking network and showed no significant intermolecular interactions at a low concentration as the distance between the aliphatic chains was larger than the van der Waals distance. However, the *n*-butylamine chains begun to aggregate and entangle when the concentration exceeded the threshold value, where the distance between the aliphatic chains was shorter than the van der Waals distance, thus forming the microphase segments that was able to insert and occupy the voids in the aromatic matrix and reduce the free volume of the system. The strong entanglement of the chains drew the network close together and reduced the distance between each segment in the matrix. As a result, the whole crosslinking network of the thermosets became compact and reinforced under this situation. However, the microphase formed by the 'defects' chains became too large for the voids in

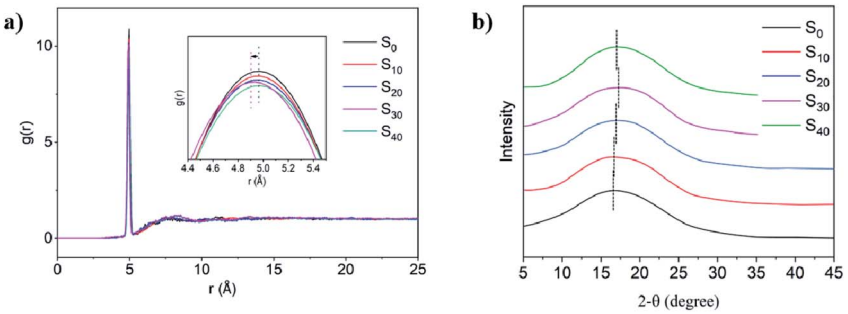

Fig. 4 (a) The RDF of all the N atoms in the system; (b) the simulated X-ray for each system.

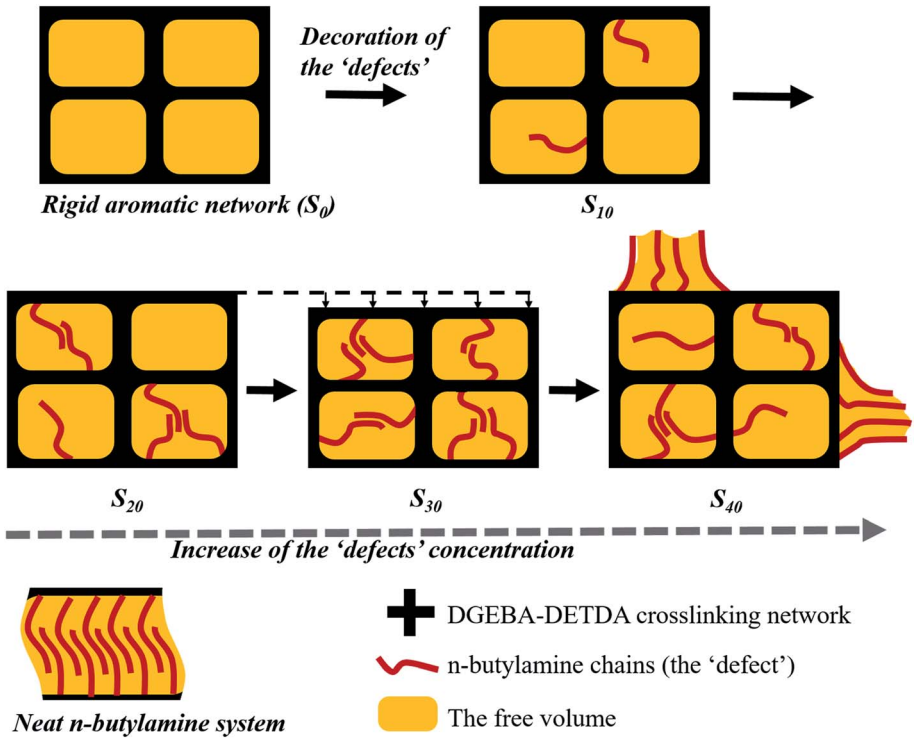

Fig. 5 Schematically demonstration of the enhancement mechanism generated by the defects in the thermosets.

the system when the proportion kept increasing, thus generating a new free volume, which, on the contrary, loosened the network structure and reduced the tensile strength of the material. At the same time, the aggregation of the 'defects' chain was promoted when the temperature was increased. The behavior of these aliphatic chains was opposite to that of the resin matrix during heating, which contributed to the reduction of T_g. The snapshots of the amorphous cells for S_0 to S_{40} at the end of the simulation were captured and are presented in the ESI section.†

Conclusions

Molecular insights into the 'defects' network in the thermosets were obtained using the MD simulation, and the influence on the mechanical properties was evaluated. The rigid aromatic DGEBA-DETDA crosslinking network structure was constructed with flexible aliphatic *n*-butylamine as the 'defects'. The simulations and experimental data in this work verified that the 'defects' in the thermosets were able to reinforce and toughen the material simultaneously. The 'defects' chains showed no intermolecular interaction at the low concentration; however, they began to aggregate and entangle when the proportion increased, where the interval between the aliphatic chains was shorter than the van der Waals distance. The microphases were generated by the aggregation and were able to insert into the voids in the matrix. The strong cohesive interaction of the entanglement reduced the distance between each segment in the matrix, making the crosslinking network compact and enhancing the moduli. The microphases kept increasing with the increase in the 'defects' concentration; however, they were no longer able to insert into the voids. A new free volume was generated by the microphases, which, on the contrary, loosened the network structure and reduced the tensile strength of the material. The results verified the fact that the low proportion 'defects' in the crosslinking network was able to reinforce and toughen the thermosets simultaneously, and clarified the corresponding mechanism. It may provide polymeric material designers a new strategy to reinforce and toughen the thermosets simultaneously without the participation of fillers.

Experimental

Amine-cured epoxy simulation systems were established using the software Materials Studio. The atomic interactions in this simulation were defined by the non-reaction force filed PCFF,[20,21] which is the typical force field used in the simulation of the epoxy resin volume change[26,27,32] with the time step set to 1 fs. A smart algorithm was employed with an energy convergence standard of 0.0001 kcal mol^{-1} and force convergence of 0.005 kcal mol^{-1} $Å^{-1}$ for the geometric optimization. During the MD simulation, the temperature was controlled by the Nose–Hoover thermostat, and the pressure was controlled by Berendsen barostat. The structures of DGEBA, DETDA, and *n*-butylamine are demonstrated in Fig. 2a. The DGEBA-DETDA backbone polymer was constructed and placed into a cubic cell; the molar ratio between each type of molecules is presented in Table 1. *n*-Butylamine molecules were manually tethered

onto the DGEBA molecules before the amorphous structure modeling as the aliphatic amine had higher reactivity than that of the aromatic amine. The initial density of the amorphous cell was preset to 1.0 g cm^{-3}, which was consistent with the experimental data[33] in order to reduce the calculated time cost by the equilibrium process. The 3D periodic boundary conditions were applied to the cubic cell, ensuring a constant atom account maintaining the system density. Subsequently, a geometry optimization based on a smart algorithm and a 50 ps *NVT* MD simulation at 300 K was performed on the initial models to rationalize the configuration. A multistep crosslinking procedure written in Perl language was performed on these equilibrated models to form the 3-D network structure.

During the ring-opening and the new bond formation processes, the secondary carbon in DGEBA and the nitrogen in DETDA were set as the reactive atoms, and the chemical reactions occurred once the reactive atoms were judged as close contact atoms in a prescribed cut-off distance. The curing conversion was increased by gradually raising the cut-off distance from 4 Å to 15 Å with an interval of 1 Å. Meanwhile, 3D equilibration cycles were adapted within every cut-off distance, thus relaxing the systems and ensuring that all the reactive atoms fully reacted under each specified cut-off distance. The crosslinking process did not stop until the final crosslinking conversion was reached or the cut-off distance was greater than the customized maximum value. Models with more than 90% conversion rate were constructed after the crosslinking process. A series of optimization processes including a geometry optimization, a 50 ps (the time step was 0.2 fs in this part specially) *NVT* MD at 300 K, a 50 ps *NVT* MD at 300 K, and a 1 ns *NPT* MD at 300 K were performed on the crosslinked models, thus eliminating the internal stress. The free volume was simulated by the calculation of the unoccupied space in the amorphous cells with the help of an atom probe ($r = 0.8$ Å).[31] The glass transition temperature (T_g) in this work was calculated by a cooling procedure, in which the structure was equilibrated by *NPT* MD for 100 ps at 550 K under atmospheric pressure, and then cooled at a rate of 10 K/50 ps from 550 K to 300 K. The T_g was determined as the inflection point of the density–temperature curve.

Conflicts of interest

All the authors declare there is no conflict of interest.

Acknowledgements

This work was supported by grants from the Science Foundation of Aeronautics of China (No. 201718S9001).

Notes and references

1 C. Y. Li and A. Strachan, *J. Polym. Sci., Part B: Polym. Phys.*, 2015, **53**(2), 103–122.
2 T. Vidil, F. Tournilhac, S. Musso, A. Robisson and L. Leibler, Control of reactions and network structures of epoxy thermosets, *Prog. Polym. Sci.*, 2016, **62**, 126–179.
3 E. M. Petrie, *Epoxy Adhesive Formulations*, 2006.
4 R. Ramsdale-Capper and J. P. Foreman, *Polymer*, 2018, **146**, 321–330.
5 R. A. Pearson and A. F. Yee, *J. Mater. Sci.*, 1991, **26**(14), 3828–3844.
6 A. F. Yee and R. A. Pearson, *J. Mater. Sci.*, 1986, **21**(7), 2462–2474.
7 Z. J. Thompson, M. A. Hillmyer, J. Liu, H.-J. Sue, M. Dettloff and F. S. Bates, *Macromolecules*, 2009, **42**(7), 2333–2335.
8 F. Meng, S. Zheng, W. Zhang, H. Li and Q. Liang, *Macromolecules*, 2006, **39**(2), 711–719.
9 E. E. Hamurcu and B. M. Baysal, *Polymer*, 1993, **34**(24), 5163–5167.
10 Y. T. Park, Y. Qian, C. Chan, T. Suh, M. G. Nejhad, C. W. Macosko and A. Stein, *Adv. Funct. Mater.*, 2015, **25**(4), 575–585.
11 F. H. Gojny, M. H. G. Wichmann, B. Fiedler and K. Schulte, *Compos. Sci. Technol.*, 2005, **65**(15), 2300–2313.
12 W. Duan, Y. Chen, J. Ma, W. Wang, J. Cheng and J. Zhang, *Composites, Part B*, 2020, **189**, 107878.
13 M. Sharifi, C. W. Jang, C. F. Abrams and G. R. Palmese, *J. Mater. Chem. A*, 2014, **2**(38), 16071–16082.
14 M. Sharifi, C. Jang, C. F. Abrams and G. R. Palmese, *Macromolecules*, 2015, **48**(20), 7495–7502.
15 L. H. Ba, Q. Zou, X. C. Tan, J. P. Song, J. Cheng and J. Y. Zhang, *RSC Adv.*, 2016, **6**(94), 91875–91881.
16 Y. Huang, Y. Tian, Y. Li, X. Tan, Q. Li, J. Cheng and J. Zhang, *RSC Adv.*, 2017, **7**(77), 49074–49082.
17 T. Yang, R. Wang, X. Hou, J. Cheng and J. Zhang, *Mater. Lett.*, 2016, **166**, 150–153.
18 B. J. Rohde, K. M. Le, R. Krishnamoorti and M. L. Robertson, *Macromolecules*, 2016, **49**(23), 8960–8970.
19 R. J. Varley, J. H. Hodgkin and G. P. Simon, *Polymer*, 2001, **42**(8), 3847–3858.
20 E. Morel, V. Bellenger, M. Bocquet and J. Verdu, *J. Mater. Sci.*, 1989, **24**(1), 69–75.
21 C. I. Vallo, P. M. Frontini and R. J. J. Williams, *Polym. Gels Networks*, 1993, **1**(4), 257–266.
22 H. Du, Z. Yang, Z. Tian, M. Huang, W. Yang, L. Zhang and A. Li, *Chem. Eng. J.*, 2018, **333**, 310–319.
23 J. Zhao, X. Liu, Z. Zhu, N. Wang, W. Sun, C. Chen and Z. He, *Appl. Surf. Sci.*, 2017, **416**, 757–765.
24 E. Yildirim, M. Yurtsever, E. Yilgör, I. Yilgör and L. Wilkes Garth, *J. Polym. Sci., Polym. Phys.*, 2017, **56**(2), 182–192.
25 E. Colangelo, Q. Chen, A. M. Davidson, D. Paramelle, M. B. Sullivan, M. Volk and R. Lévy, *Langmuir*, 2017, **33**(1), 438–449.
26 S. Yang and J. Qu, *Polymer*, 2012, **53**(21), 4806–4817.
27 I. Yarovsky and E. Evans, *Polymer*, 2002, **43**(3), 963–969.
28 V. Varshney, S. S. Patnaik, A. K. Roy and B. L. Farmer, *Macromolecules*, 2008, **41**(18), 6837–6842.
29 C. Li and A. Strachan, *Polymer*, 2015, **75**, 151–160.
30 S. Masoumi, B. Arab and H. Valipour, *Polymer*, 2015, **70**, 351–360.
31 C. Li and A. Strachan, *Polymer*, 2016, **97**, 456–464.
32 H. B. Fan and M. M. F. Yuen, *Polymer*, 2007, **48**(7), 2174–2178.

33 D. Ratna, R. Varley, R. K. S. Raman and G. P. Simon, *J. Mater. Sci.*, 2003, **38**(1), 147–154.
34 K. Li, Y. Li, Q. Lian, J. Cheng and J. Zhang, *J. Mater. Sci.*, 2016, **51**(19), 9019–9030.
35 Z. Wang, Q. Lv, S. Chen, C. Li, S. Sun and S. Hu, *ACS. Appl. Mater. Interfaces*, 2016, **8**(11), 7499–7508.
36 Z. K. Wang, Q. Lv, S. H. Chen, C. L. Li, S. Q. Sun and S. Q. Hu, *Mol. Simul.*, 2015, **41**(18), 1515–1527.